Neutron-scattering study of metallic sodium

H. Abe, K. Ohshima, T. Suzuki, and S. Hoshino
Institute of Applied Physics, University of Tsukuba, Tsukuba 305, Japan

K. Kakurai
Institute for Solid State Physics, The University of Tokyo, Roppongi, Minato-ku, Tokyo 106, Japan
(Received 29 March 1993; revised manuscript received 27 September 1993)

A neutron elastic- and inelastic-scattering study has been performed on single crystals of metallic sodium over a temperature range of 10 to 300 K. On cooling the virgin sample, the incubation time to transform from the bcc structure to the low-temperature structure was found to be more than 2 h at 38 K. The full width at half maximum (FWHM) of the $(110)_{bcc}$ Bragg reflection suddenly increased from 0.3° to 0.73°, due to some deformation introduced by the nucleation of the low-temperature structure. In relation to the deformation, strong extra-diffuse scattering was observed around the $(110)_{bcc}$ Bragg reflection in addition to thermal diffuse scattering. On warming through the transformation, the FWHM gradually recovered but was larger than that of the virgin state. Apparently some deformation still remained in the bcc structure even though the low-temperature structure disappeared. It was estimated that the cluster size of the low-temperature phase is more than 3.2 nm along the c axis from analyzing the Huang-type diffuse scattering. On cooling again, the phase transition did not take place until 10 K and a waiting time of at least 20 min at that temperature was needed before the transformation took place. No drastic change in the $TA_1[110]$ phonon-dispersion branch down to 38 K was observed, though the phonon energies for $q \geq 0.25$ decreased slightly with decreasing temperature.

I. INTRODUCTION

Many studies of martensitic phase transition have been performed for binary and ternary alloys to understand the peculiar structural change. The phase-transition temperature strongly depends on the composition. As the composition fluctuation is playing a role in the alloys, the mechanism of phase transition will be of a more complicated nature. It is, therefore, of importance to study the microscopic structure change in elements, in particular, alkali metals, for understanding the nature of the proper martensitic phase transition.

Barrett[1] found that metallic sodium partially undergoes martensitic phase transition from body-centered-cubic (bcc) structure to a close-packed hexagonal structure with stacking faults on cooling (below 36 K, M_s). It has a hysteresis whose inverse transformation temperature is 78 K (A_s). The low-temperature phase has recently been proposed to be the 9R structure, i.e., ABCBCACAB stacking sequence, whose volume fraction was determined to be 43% by a neutron powder diffraction study.[2] In addition, an investigation on phonon softening in the lowest branch $TA_1[110]$ was performed between 230 and 40 K by Blaschko and Krexner.[3] They mention that the frequencies near the zone boundary decrease by an amount of about 4%. An experimental and theoretical study of the phase transition in sodium under pressure was made by Vaks *et al.*[4] They explained why the transition temperature decreased with increasing pressure. Very recently, two reports on the structure of metallic sodium have appeared consecutively. Berliner *et al.*[5] have found no evidence of transformation precursors above M_s in the measurements of the diffuse scattering, diffraction line widths, quasielastic scattering, and the temperature dependence of the $\Sigma_4[hh0]$ phonon energies with the use of neutron-diffraction and neutron inelastic-scattering techniques. They have also indicated that the low-temperature structure of metallic sodium is a complex mixture of rhombohedral polytypes, forming a ladder of structures related by specific stacking faults. Schwarz, Blaschko, and Gorgas[6] have proposed the presence of two long-range-ordered, but faulted hcp and 9R structures.

Metallic lithium also shows the martensitic phase transition from the bcc structure to the 9R structure near 74 K. Twin $(009)_{9R}$ Bragg reflections were displaced from 4° from the $(110)_{bcc}$ Bragg reflection below M_S.[7] Moreover, Smith[8] found that it took a few minutes to transform into the low-temperature phase at constant temperature. After this delay time, the full width at half maximum (FWHM) of the $(100)_{bcc}$ Bragg reflection increases from 0.5° to 1.2°. Gooding and Krumhansl[9] presented a Landau theory of the phase transition in metallic lithium and proposed that the transition occurs via incomplete softening of the $(\frac{1}{3}, \frac{1}{3}, 0)$ Σ_4 phonon. Pressure effects on the phase transition in polycrystalline lithium have been investigated by high-resolution neutron-diffraction experiments.[10] It was found that the 9R phase transformed into the fcc phase over a narrow temperature range near 140 K on warming at 6.5 kbar. Static and dynamic precursor phenomena of the lattice instability of metallic lithium were also investigated by elastic- and inelastic-neutron-scattering experiments.[11] Extra diffuse scattering around the $(200)_{bcc}$ Bragg reflection was observed in a deteriorated single crystal. A softening of the $TA_1[110]$ branch at the zone boundary was also found. In metallic potassi-

0163-1829/94/49(6)/3739(7)/$06.00

um, however, neutron-diffraction[12] and synchrotron x-ray studies[13] do not yield a martensitic phase transition down to 5 and 10 K, respectively. In these three elements, we need more microscopic and systematic studies prior to and posterior to the onset of the transition. We have started such a study choosing metallic sodium as the specimen.

Both neutron elastic- and inelastic-scattering experiments from metallic sodium have been performed to observe the temperature dependence of a phonon-dispersion curve in the $TA_1[110]$ branch and the temperature dependence of the FWHM from the $(110)_{bcc}$ Bragg reflection. Diffuse scattering near the $(110)_{bcc}$ Bragg reflection was also measured.

II. EXPERIMENT

Three spherical single crystals were prepared in liquid paraffin above the melting point of sodium (97 °C) and gradually cooled down to room temperature. The sizes of the specimens used in this experiment were 5, 10, and 18 mm in diameter. Rocking curves of the $(110)_{bcc}$ Bragg reflection for the three specimens were measured and the mosaic spread of the specimens was about 20 min. These specimens were kept in an aluminum container filled with pure helium gas. The neutron-scattering experiments were performed with the use of the triple-axis spectrometer of the Institute for Solid State Physics, The University of Tokyo, installed at beamline 5G of the JRR-3M research reactor in the Japan Atomic Energy Research Institute, Tokai, Japan. Pyrolytic graphite (PG) was used both as a monochromator and as an analyzer. The $\lambda/2$ contamination was suppressed by a PG filter in front of the monochromator. The collimations before the monochromator, before and after the sample, and after the analyzer were 60, 40, 40, and 40 min, respectively. The scattering data were collected between room temperature and 10 K with the use of a closed-cycle refrigerator. The measurement of inelastic-scattering intensity was done at a constant incident-neutron wavelength (0.235 nm), where energy resolution was 0.87 meV. The temperature of the specimen was controlled with an accuracy of 0.1°.

III. RESULTS AND ANALYSIS

A. Phonon-dispersion curve in the $TA_1[110]$ branch

A phonon-dispersion curve in the $TA_1[110]$ branch was measured in detail for the 18 mm sample, from 200 to 38 K before the transformation. Figure 1 shows the phonon-dispersion curve of the $TA_1[110]$ branch at 200 and 38 K. We have also plotted relative phonon energy shifts, $\Delta E/E$ vs temperature in Fig. 2. As it was difficult to separate an elastic component from the energy spectrum, error bars were larger in the small q region than those near the zone boundary. The phonon-dispersion curve in the present experiment is in good agreement with the result of Berliner *et al.*[5] As the zone boundary is approached, the phonon energies decreased slightly with decreasing temperature.

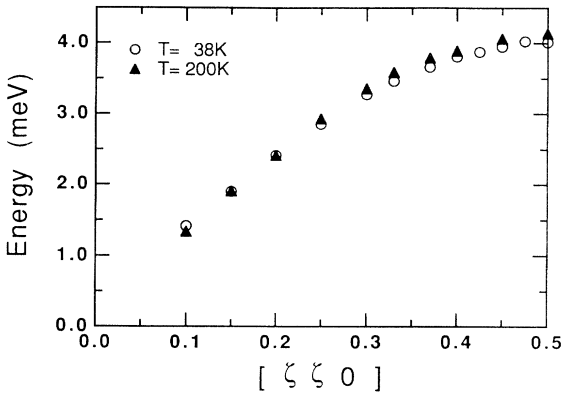

FIG. 1. Phonon-dispersion curve of the $TA_1[110]$ branch at 200 K (▲) and 38 K (○).

B. FWHM of $(110)_{bcc}$ Bragg reflection

To obtain the temperature dependence of the FWHM for the $(110)_{bcc}$ Bragg reflection, two steps of a temperature cycle were used; in the first step, the specimen was cooled from 200 down to 38 K and then heated up to 90 K, and in the second step, it was cooled from 90 down to 10 K and then heated up to 200 K again. A schematic diagram of the temperature is shown in Fig. 3. In the first cycle, no structural change was seen after the tem-

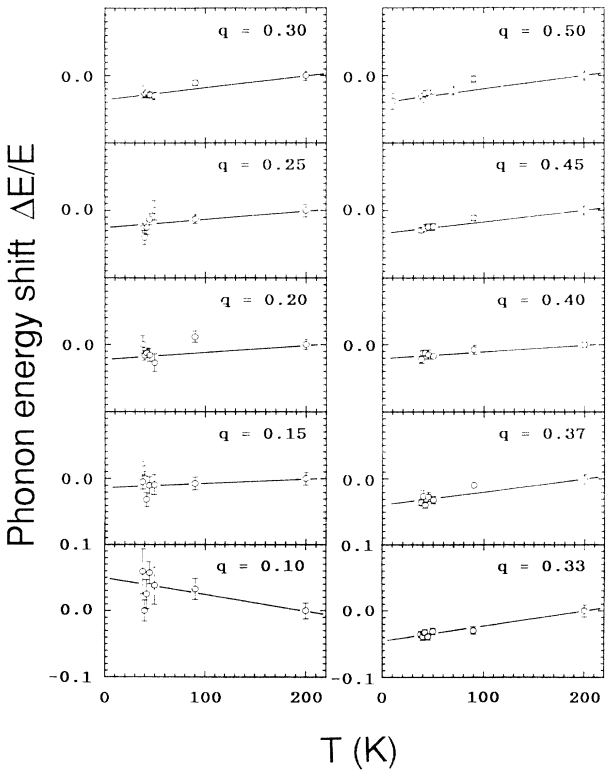

FIG. 2. Relative phonon energy shifts $\Delta E/E$ vs temperature for phonons of the $TA_1[110]$ branch.

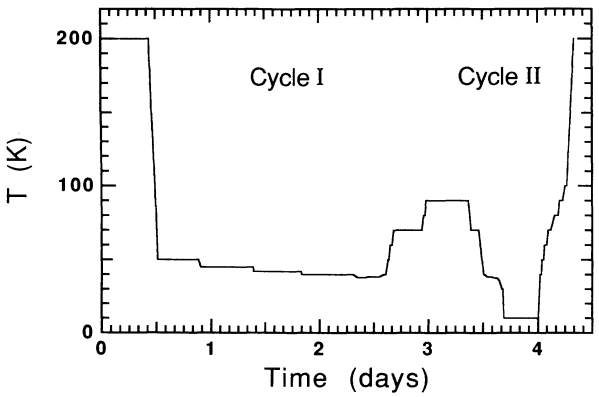

FIG. 3. Schematic drawing of the temperature cycle.

perature reached 38 K. While the temperature was kept constant, some parts of the parent phase were suddenly transformed into the low-temperature phase more than 2 h later; we call this delay period the incubation time. Figure 4 shows the time dependence of the FWHM for the $(110)_{bcc}$ Bragg reflection at 38 K. The FWHM had increased to 0.73° discontinuously. Such an abrupt increase of the FWHM indicates that some deformation was introduced in the parent phase, resulting from the nucleation of the low-temperature structure. The same change of FWHM of the $(110)_{bcc}$ reflection was found after the transformation in the studies by Berliner *et al.*[5] and Schwarz, Blaschko, and Gorgas.[6] After the incubation time, two weak Bragg reflections and strong diffuse scattering were observed in addition to the $(110)_{bcc}$ Bragg reflection and the thermal diffuse scattering (TDS). The equi-intensity distribution in the $(hk0)$ reciprocal-lattice plane is shown in Fig. 5. The positions of the two Bragg reflections are the same as those in metallic lithium as described in the Introduction (Fig. 2 of Ref. 7). Therefore, we assign them as $(009)_{9R}$. In this experiment, we have not attempted to determine the low-temperature structure in further detail. Temperature dependence of diffuse scattering will be described in Sec. III C in detail. Figure 6 shows the temperature dependence of the FWHM of

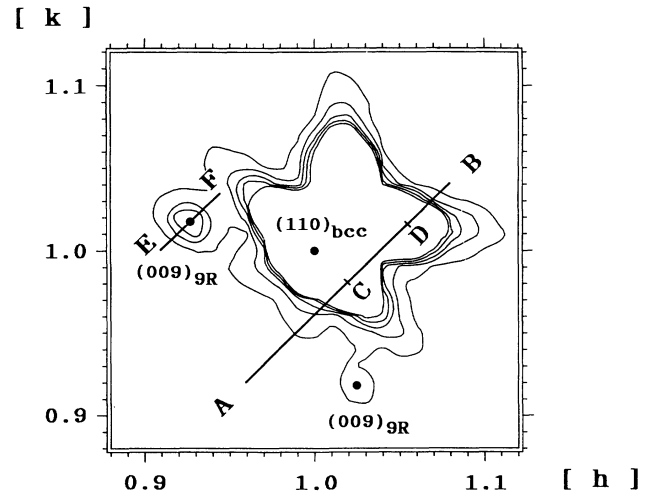

FIG. 5. Equi-intensity distribution in the $(hk0)$ reciprocal-lattice plane including $(110)_{bcc}$ and $(009)_{9R}$ Bragg reflections. Line AB and two marks, C and D, are shown for reference in Fig. 8. Line EF is also shown for reference in Fig. 7.

the $(110)_{bcc}$ Bragg reflection. The FWHM of the $(110)_{bcc}$ Bragg reflection gradually decreased from 50 K and did not change near 70 K on further warming. At the same time, the $(009)_{9R}$ Bragg reflection disappeared at around 70 K. Taking into account the temperature change in the FWHM for the $(110)_{bcc}$ Bragg reflection, an inverse transformation temperature of this specimen was determined to be about 70 K. It is clear that the FWHM of the $(110)_{bcc}$ Bragg reflection at this temperature was larger than that for an initial state. Some deformation still remained in the bcc structure even though the low-temperature structure disappeared.

In the second temperature cycle, the martensitic transformation did not take place until 10 K while the temperature decreased at the rate of 10.7 K/h as shown in Fig. 3. At 10 K, an incubation time of at least 20 min was observed. On warming again, the inverse transformation

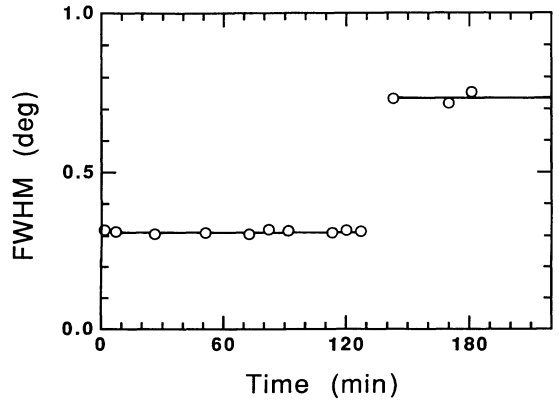

FIG. 4. FWHM of the $(110)_{bcc}$ Bragg reflection vs time at $T=38$ K.

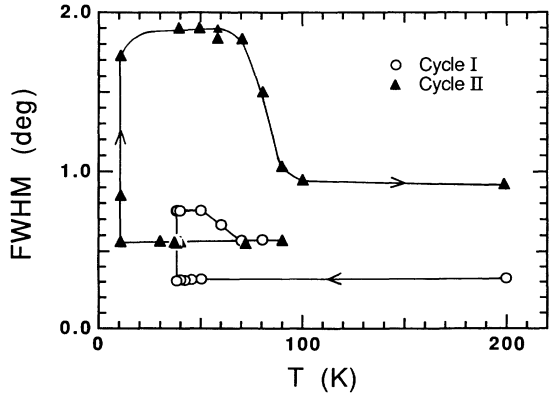

FIG. 6. Temperature dependence of FWHM for the $(110)_{bcc}$ Bragg reflection. (○) First temperature cycle (200→38→90 K) and (▲) second temperature cycle (90→10→200 K).

took place between 70 and 90 K. The residual value of the FWHM in the second temperature cycle was large compared with that in the first temperature cycle. This was considered as being due to an increase in the extrinsic deformation.

Figure 7 shows the temperature dependence of the intensity of the $(009)_{9R}$ Bragg reflection along the line EF in Fig. 5. As described above, the $(009)_{9R}$ Bragg reflection appeared suddenly at 38 K after the incubation time and vanished at 70 K on warming. In the second temperature cycle, the $(009)_{9R}$ Bragg reflection appeared at 10 K and vanished at around 80 K.

C. Diffuse scattering around the $(110)_{bcc}$ Bragg reflection

As shown in Fig. 5, the peculiar diffuse scattering appeared near the $(110)_{bcc}$ Bragg reflection in addition to TDS after the phase transition. We can classify the scattering as symmetrical diffuse scattering along the $\langle 1\bar{1}0 \rangle$ direction and asymmetrical diffuse streaks with an elongation in the [100] and [010] directions. Hereafter, we call the latter extra-diffuse scattering (EDS). As the intensity distribution of the former is similar to Huang-type diffuse scattering due to the size-effect modulation, it is called HDS. The temperature dependence of the intensity distribution in the first termperature cycle along the line AB in Fig. 5 is shown in Fig. 8. From the figure, weak diffuse scattering appeared at point *C* before the phase-transition temperature (> 38 K). This is not due to localized diffuse scattering precursors of the martensitic transformation but to regular thermal diffuse scattering (TDS), which is independent of phase transition and is gradually decreasing with decreasing temperature. The intensity ratio between TDS and EDS is estimated to be about one-tenth at 38 K. On warming, the diffuse intensity maximum at *C* decreased gradually with increasing temperature and became almost constant at 70 K. The diffuse intensity maximum at D became constant with increasing temperature, drastically decreased around 70 K; and vanished at 80 K. The major part of the intensity maximum at C contains EDS+HDS, even if TDS increases with increasing temperature. In the second temperature cycle, the diffuse maximum at C became almost constant down to 10 K before the phase transformation on cooling, and suddenly increased after the phase transformation at 10 K, as shown in Fig. 8. The intensity maximum at D is much smaller than that at C and the intensity maximum at D is shifted toward C, compared

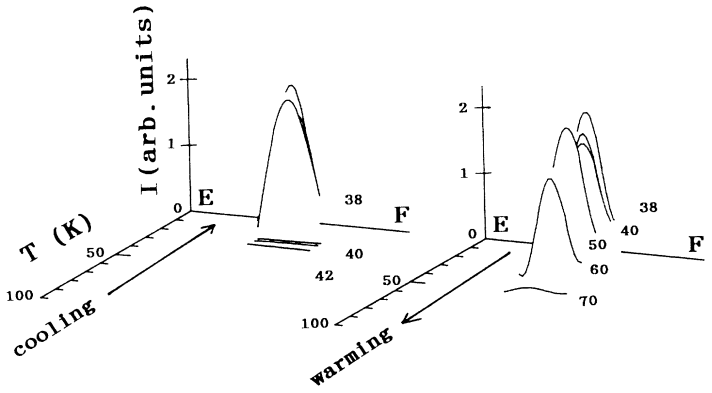

Cycle I

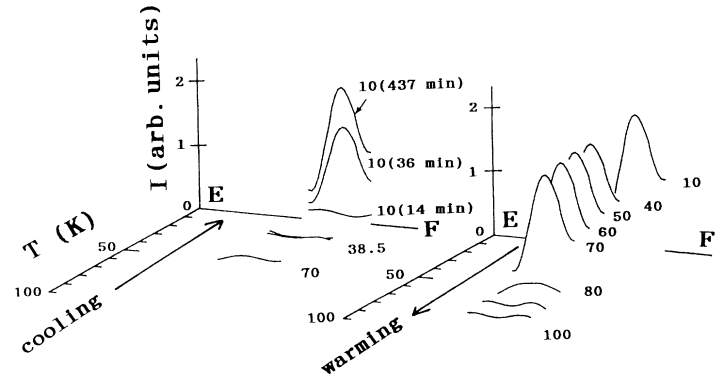

Cycle II

FIG. 7. Temperature dependence of intensity for the $(009)_{9R}$ Bragg reflection along the line EF in Fig. 5. Cycle I: first temperature cycle (42→38→70 K); and cycle II: second temperature cycle (70→10→100 K).

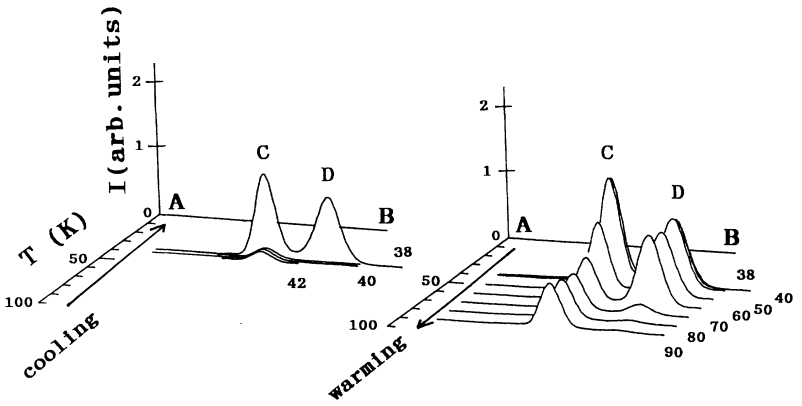

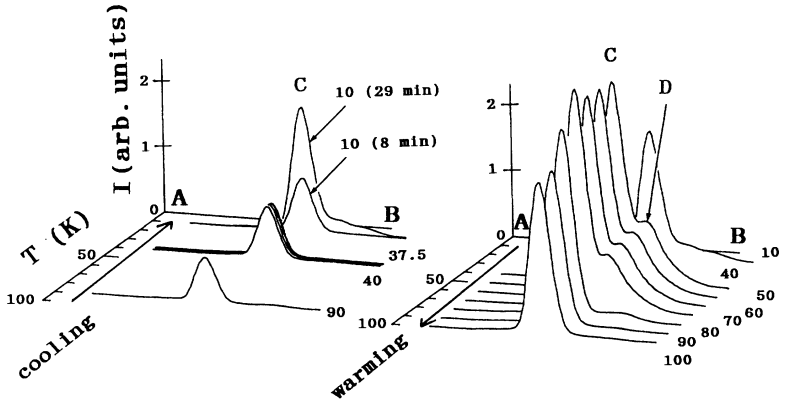

FIG. 8. Temperature dependence of diffuse scattering intensity distribution along the line AB in Fig. 5. Marks C and D are the same points as shown in Fig. 5. Cycle I: first temperature cycle (42→38→70 K), and cycle II: second temperature cycle (70→10→100 K).

with the relation in cycle I. On warming, the intensity maximum at C increased a little at 40 K, became almost constant up to 70 K, and decreased a little at 90 K. On the other hand, the intensity maximum at D increased a little at 40 K, became almost constant up to 70 K, drastically decreased at 80 K, and disappeared at 90 K.

Schwarz, Blaschko, and Gorgas[11] reported the diffuse scattering in a deteriorated single crystal of metallic lithium at 100 K, whose pattern shows intensity streaks along the [110] directions and indicates the presence of a static $[110]\langle 1\bar{1}0\rangle$ shear distortion in the crystal. In metallic sodium, the origin of the diffuse intensity at C in Fig. 5 is understood to come from the internal strains in the parent phase after the phase transformation, because EDS still exists at 90 K and its intensity in the second temperature cycle is much large than that observed in the first temperature cycle, as shown in Fig. 8. This behavior bears a strong resemblance to the temperature dependence for the FWHM of the $(110)_{bcc}$ Bragg reflection in Fig. 6. On the other hand, the origin of the diffuse intensity at D is assigned to the local distortion around the boundary between the parent and low-temperature phases or distortion in the low-temperature phase, because the intensity disappears at the inverse transition temperature. There are several methods to analyze the diffuse intensities quantitatively. One of them was developed by Dederichs,[14] who introduced three types of imperfections (substitutional impurities, vacancies, and interstitial atoms) contributing to the structural fluctuations, and formulated the diffraction theory. We summarize relevant intensity formulas briefly for reference. The diffusely scattered intensity from defect crystals is given as

$$I_{\text{diff}} \propto b^2 \left| \sum_n [1+\exp(i\mathbf{K}\cdot\mathbf{r}_n)\{\exp(i\mathbf{K}\cdot\mathbf{u}_n)-1\}] \right|^2 , \quad (1)$$

were b is the scattering amplitude of sodium atom, $\mathbf{K}$ is the scattering vector, and $\mathbf{u}_n$ is the displacement vector from the nth bcc lattice site $\mathbf{r}_n$. The overall form of the diffuse scattering intensity I_{diff} near the Bragg reflection can be identified in the so-called Huang and asymptotic regions for which

$$I_{\text{diff}} \propto (Kq^{-1})^2, \quad q \ll 1/R, \quad \text{Huang scattering} , \quad (2)$$

$$I_{\text{diff}} \propto (KR^2q^{-4}), \quad q > 1/R ,$$

asymptotic (or Stokes-Wilson) scattering , (3)

where the scattering vector $\mathbf{K}$ specifies the measuring po-

sition in reciprocal space in terms of the reciprocal-lattice vector **h**, a vector **q** relative to **h**, and R is the size of clusters. The asymptotic scattering region falling off as the inverse fourth power of q is characterized by local Bragg scattering from the highly distorted lattice near the clusters. There the size of the clusters can be estimated from measuring the diffuse intensity variation along a specified q direction.

We have tried to obtain the cluster size of the low-temperature phase along the stacking sequence after analyzing HDS. To separate HDS from the total scatterings, it is assumed that the intensity distributions at each temperature are given as

$$I(40\ \mathrm{K})=I^{\mathrm{Bragg}}+I^{\mathrm{TDS}} \text{ before transition ,}$$

$$I(38\ \mathrm{K})=I^{\mathrm{Bragg}}+I^{\mathrm{TDS}}+I^{\mathrm{EDS}}+\mathrm{I}^{\mathrm{HDS}} \text{ after transition ,}$$

and

$$I(70\ \mathrm{K})=I^{\mathrm{Bragg}}+I^{\mathrm{TDS}}+I^{\mathrm{EDS}}$$

just after inverse transition .

In consideration of an extinction effect, we have normalized them with the use of the $(110)_{\mathrm{bcc}}$ Bragg intensity (I^{Bragg}) at each temperature. I^{TDS} was also corrected with the use of the standard form (see Chap. 11 of Ref. 15). We assume that EDS has no temperature variation even though HDS disappears at the inverse transition temperature. $\mathrm{I}^{\mathrm{HDS}}$ is, thus, obtained from the intensity difference between $I(38\ \mathrm{K})$ and $I(70\ \mathrm{K})$. Figure 9 shows the intensity distribution I^{HDS} at 38 K thus obtained. It is similar to the typical Huang-type diffuse scattering. The diffuse intensity at $(110)_{\mathrm{bcc}}$ reflection was plotted along the $[1\bar{1}0]$ direction and shown in Fig. 10. In the figure, the q^{-4} region is found above $q=0.03$, although the q^{-2} region is not found in the vicinity of small q due to the limitation of neutron-resolution function. We have

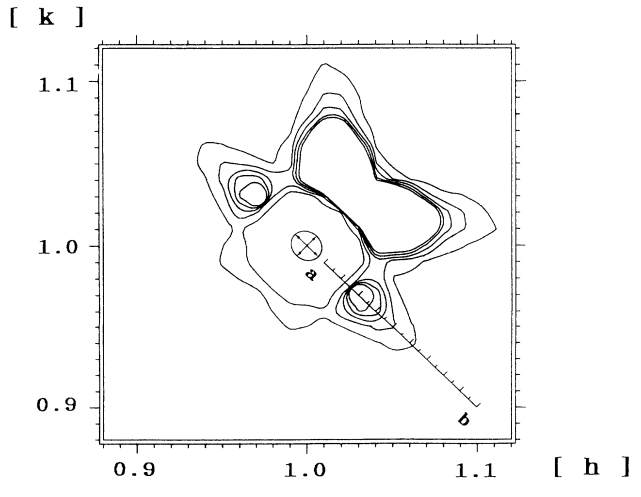

FIG. 9. Intensity distribution of Huang-type diffuse scattering I^{HDS} at 38 K on the $(hk0)$ plane. Central circle means two-dimensional distribution at half maximum of the intensity for the $(110)_{\mathrm{bcc}}$ Bragg reflection. The line is shown for reference in Fig. 10.

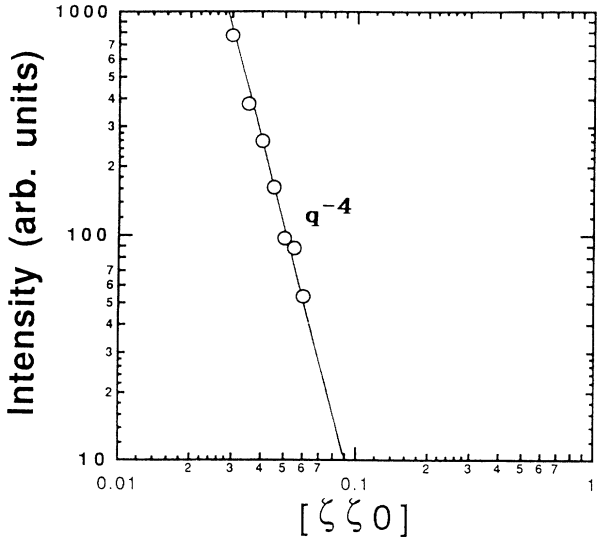

FIG. 10. Intensity I^{HDS} vs reduced wave vector $\zeta=qa_0/\sqrt{2}\pi$ at $(110)_{\mathrm{bcc}}$ along the $[1\bar{1}0]$ direction, where a_0 is the lattice parameter of the bcc structure. The line measured is depicted in Fig. 9.

estimated from the q^{-4} dependence of I^{HDS} along the $[1\bar{1}0]$ direction that the cluster size of the low-temperature phase along the stacking sequence is more than 3.2 nm.

We have also tried to perform the model calculation of diffuse scattering that appeared at point D to understand the local structure and compare it with observed intensity distribution. The clusters described above affect their neighboring atoms in the parent phase with displacements from the regular positions. The diffuse intensity on the $(hk0)$ plane, expressed by Eq. (1), is fitted to the observed one by the Monte Carlo simulation method. Figure 11 shows the simulated intensity distribution, in which the displacement vector $\mathbf{u}_n$ is directed several degrees off from the [110] direction. If the volume change

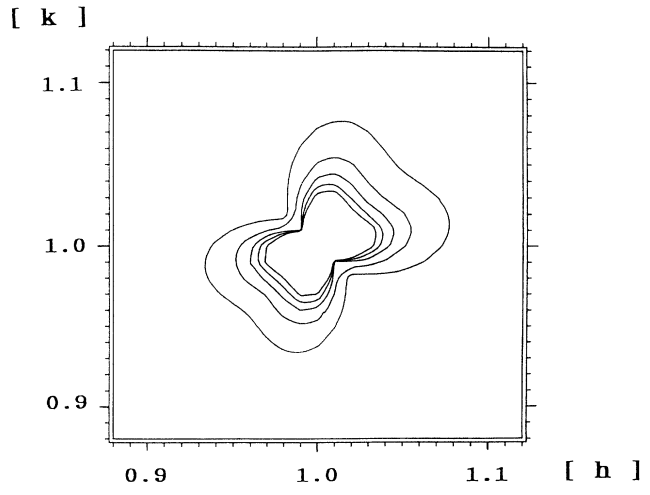

FIG. 11. Intensity distribution calculated by Eq. (1) in the text on the $(hk0)$ plane. Compare it with Fig. 9

of the bcc unit cell is introduced in the intensity formula, the asymmetric diffuse pattern along the [110] direction is obtained and becomes similar to the observed pattern. Although this is a tentative and simple model, it offers the possibility of modifications of the diffuse intensity distribution by the displacement and the volume change in the parent phase, which decrease with the distance from clusters.

IV. REMARKS

The present work has yielded the following important information on the martensitic phase transition in metallic sodium. First, a delay time, so-called incubation time, of more than 2 h is needed for the transformation into the low-temperature phase at 38 K in metallic sodium, while it takes only a few minutes at 72.3 K in metallic lithium.[8] It is thought that the incubation time is an essential feature of martensitic phase transition in alkali metals. We might observe a martensitic phase transition in metallic potassium after a long incubation time at very low temperature. Second, in the second cycle, the martensitic phase-transition temperature M_s appears at a lower temperature than that of the first cycle (38 K). The deformation in the crystal has to influence the critical temperature of the phase transition. Third, we have estimated the cluster size of the low-temperature phase by analyzing the Huang-type diffuse scattering. More detailed information on the structural information would be obtained with the use of a high-resolution neutron source and four-axis spectrometer.

ACKNOWLEDGMENTS

The authors would like to thank Dr. Y. Watanabe of Tohoku University for much help in taking preliminary x-ray experiments and Dr. T. Kakeshita of Osaka University for helpful discussions. This study was supported by a Grant-in-Aid for Scientific Research (No. 02402045) and a Grant-in-Aid for Cooperative Research (No. 04302053) from the Ministry of Education, Science, and Culture, and a Monbusho International Scientific Research Program (No. 04044032). Additional support was provided by the Murata Science Foundation (No. 911109) and the University of Tsukuba Research Project.

[1]C. S. Barrett, Acta Crystallogr. **9**, 671 (1956).
[2]R. Berliner, O. Fajen, H. G. Smith, and R. L. Hitterman, Phys. Rev. B **40**, 12 086 (1989).
[3]O. Blaschko and G. Krexner, Phys. Rev. B **30**, 1667 (1984).
[4]V. G. Vaks, M. I. Katsnelson, V. G. Koreshkov, A. I. Likhtenstein, O. E. Parfenov, V. F. Skok, V. A. Suhhoparov, A. V. Trefilov, and A. A. Chernyshov, J. Phys. Condens. Matter **1**, 5319 (1989).
[5]R. Berliner, H. G. Smith, J. R. D. Copley, and J. Trivisonno, Phys. Rev. B **46**, 14 436 (1992).
[6]W. Schwarz, O. Blaschko, and I. Gorgas, Phys. Rev. B **46**, 14 448 (1992).
[7]G. Ernst, C. Artner, O. Blaschko, and G. Krexner, Phys. Rev. B **33**, 6465 (1986).
[8]H. G. Smith, Phys. Rev. Lett. **58**, 1228 (1987).
[9]R. J. Gooding and J. A. Krumhansl, Phys. Rev. B **38**, 1695 (1988).
[10]H. G. Smith, R. Berliner, J. D. Jorgenson, M. Nielsen, and J. Trivisonno, Phys. Rev. B **41**, 1231 (1990).
[11]W. Schwarz, O. Blaschko, and I. Gorgas, Phys. Rev. B **44**, 6785 (1991).
[12]L. Pintschovius, O. Blaschko, G. Krexner, M. de Podesta, and R. Currat, Phys. Rev. B **35**, 9330 (1987).
[13]H. You, J. D. Axe, D. Hohlwein, and J. B. Hastings, Phys. Rev. B **35**, 9333 (1987).
[14]P. H. Dederichs, J. Phys. F **3**, 471 (1973).
[15]B. E. Warren, *X-Ray Diffraction* (Addison-Wesley, Reading, MA, 1969).